Proceedings of the EuroGNC 2013, 2nd CEAS Specialist Conference on
Guidance, Navigation & Control, Delft University of Technology, Delft,
The Netherlands, April 10-12, 2013

A Spherical Coordinate Parametrization for an In-Orbit Bearings-Only Navigation Filter

J. Grzymisch, W. Fichter, M. Casasco and D. Losa

Abstract In-orbit rendezvous is a key enabling technology for many space missions. Implementing it employing only bearing measurements would simplify the relative navigation hardware currently required, increasing robustness and reliability by reducing complexity, launch mass and cost. The problem of bearings-only navigation has been studied intensively by the Naval and Military communities. Several authors have proposed that a polar or spherical coordinate parametrization of the underlying dynamics produces a more robust navigation filter due to the inherent de-coupling of the observable and un-observable states. Nevertheless, the complexity of this problem increases significantly when the underlying dynamics follow those of relative orbital motion. This paper develops a spherical coordinate parametrization of the linearized relative orbital motion equations for elliptical orbits and uses an approximation of these equations for circular orbits to develop an Extended Kalman Filter (EKF) for bearings-only navigation. The resulting filter is compared to its equivalent based on the well known Hill Equations in cartesian coordinates via a Monte Carlo analysis for a given reference trajectory. Simulations show that a spherical coordinate based EKF can perform better than its cartesian coordinate counterpart in terms of long-term stability tracking of the reference trajectory, with little additional computational effort.

Jonathan Grzymisch
Institute of Flight Mechanics and Control, University of Stuttgart, Germany.
e-mail: jonathan.grzymisch@ifr.uni-stuttgart.de

Prof. Walter Fichter
Institute of Flight Mechanics and Control, University of Stuttgart, Germany.

Massimo Casasco
European Space Technology Centre, European Space Agency, The Netherlands.

Damiana Losa
Research and Technology Department, Thales Alenia Space, France

1 Introduction

In-orbit rendezvous is a key enabling technology for many space missions. Without a technology allowing a chaser spacecraft to reach a target with high accuracy and low collision risk, we could never achieve missions such as in-orbit assembly of large structures (ISS); planetary exploration and return (Apollo and Mars Sample Return); in-orbit servicing, refuelling and inspection (ATV, DEOS) and Active de-orbiting (OTV).

While this topic has been widely researched and there exists significant heritage, it currently requires complex and/or bulky hardware to measure the relative range between the chaser spacecraft and the target [1]. This is especially the case with un-cooperative targets at long distances, as the power requirements and complexity of the range sensors increases exponentially without dedicated hardware on the target [2]. There have been may efforts to simplify the required hardware for rendezvous [1]. Nevertheless, most solutions only work at short ranges of less than a few kilometres, such as those involving visual cameras using stereo vision (triangulation along a well-known baseline) or estimation of the range from the relative size of the target.

For these reasons there is a strong motivation to develop algorithms to perform in-orbit rendezvous without requiring a direct measurement of the range between the chaser and the target. Bearing measurements to an un-cooperative target are easier to obtain, especially at long range, without the need of heavy or complex hardware, for example by using a single optical camera to measure Line of Sight to the target. Therefore, this would not only enable rendezvous missions with low launch mass and cost, but would also provide a back-up strategy for contingency cases in missions employing more advance sensors.

The problem of bearings-only navigation has been studied intensively by the Naval and Military communities with applications to ship navigation and missile guidance assuming a constantly moving and non-maneuvering target [3–5]. In particular, there have been several studies claiming that using a polar or spherical coordinate parametrization of the equations of motion to construct an EKF for bearings-only navigation naturally decouples the un-observable states (range) from the observable ones (angles). This prevents covariance matrix ill-conditioning and filter instability, resulting in a more robust and unbiased filter [6, 7].

Nonetheless, the assumptions employed in the Naval and Military literature do not apply to the in-orbit problem due to the complexity of orbital dynamics. Only a few authors have treated the in-orbit bearings-only navigation problem [1] and to the authors' knowledge, none have attempted to test the potential advantages of a spherical coordinate parametrization for a bearings-only navigation filter for in-orbit rendezvous. This paper tackles this specific problem and for this purpose develops a spherical coordinate parametrization for the equations of linearized relative orbital motion for eccentric and circular orbits. The latter are equivalent to the well known Hill Equations.

2 Spherical Relative Motion Equations

In order to derive the equations of relative motion in Spherical coordinates, the definition of the relative position vector in spherical coordinates (see Appendix) is used in conjunction with the vectorial equation of relative motion (16) derived in the Appendix. Solving for the desired accelerations in Spherical coordinates $\ddot{r}$, $\ddot{\theta}$ and $\ddot{\phi}$, the final expressions for the Spherical Equations of Relative Motion emerge and are shown in Equations 1 to 3. These equations are valid for elliptical orbits.

$$\begin{aligned}\ddot{r} = {} & a_r + \dot{\phi}^2 r + r\omega^2 + 2kr\omega^{\frac{3}{2}} + r\dot{\theta}^2 c_\phi^2 - r\omega^2 c_\phi^2 + r\omega^2 c_\phi^2 c_\theta^2 - 3kr\omega^{\frac{3}{2}} c_\phi^2 \dots \\ & + 2\dot{\phi} r\omega c_\theta + 2r\dot{\theta}\omega s_\theta c_\phi s_\phi\end{aligned} \tag{1}$$

$$\ddot{\theta} = \frac{a_\theta - 2\dot{r}\omega s_\phi s_\theta}{r c_\phi} + \frac{2\dot{\phi}\dot{\theta} s_\phi - \dot{\omega} s_\phi s_\theta}{c_\phi} - \frac{2\dot{r}\dot{\theta}}{r} - c_\theta s_\theta \omega^2 - 2\dot{\phi} s_\theta \omega \tag{2}$$

$$\begin{aligned}\ddot{\phi} = {} & -\dot{\omega} c_\theta - \dot{\theta}^2 s_\phi c_\phi + \omega^2 s_\phi c_\phi s_\theta^2 + \frac{a_\phi - 2\dot{\phi}\dot{r} - 2\dot{r}\omega c_\theta}{r} + 3k\omega^{\frac{3}{2}} s_\phi c_\phi \dots \\ & + 2\dot{\theta}\omega s_\theta c_\phi^2\end{aligned} \tag{3}$$

Here $c_i = \cos(i)$ and $s_i = \sin(i)$ for $i = \phi$ or θ are used to simplify the notation. Substituting the assumptions of constant orbital rate $\omega = \sqrt{\mu / r_t^3}$ into Equations 1 to 3, yields the Equations for Relative Motion in Spherical Coordinates for Circular Orbits, shown in Equations 4 to 6. These are equivalent to the Hill Equations cited in many references including [2], also shown in the Appendix.

$$\ddot{r} = a_r + r\dot{\phi}^2 + 2r\dot{\phi}\omega c_\theta + r\dot{\theta}^2 c_\phi^2 + 2r s_\phi s_\theta \dot{\theta}\omega c_\phi + r\omega^2 \left(c_\phi^2 c_\theta^2 - 4c_\phi^2 + 3\right) \tag{4}$$

$$\ddot{\theta} = \frac{a_\theta - 2\dot{r}\omega s_\phi s_\theta}{r c_\phi} + \frac{2\dot{\phi}\dot{\theta} s_\phi}{c_\phi} - \frac{2\dot{r}\dot{\theta}}{r} - c_\theta s_\theta \omega^2 - 2\dot{\phi} s_\theta \omega \tag{5}$$

$$\ddot{\phi} = \frac{a_\phi - 2\dot{\phi}\dot{r} - 2\dot{r}\omega c_\theta}{r} + \omega^2 s_\phi c_\phi \left(s_\theta^2 + 3\right) - \dot{\theta}^2 s_\phi c_\phi + 2\dot{\theta}\omega s_\theta c_\phi^2 \tag{6}$$

3 Validation of the Spherical Equations

In order to validate the equations of relative motion for circular orbits in Spherical coordinates, a comparison of equations 4 to 6 with the Hill Equations (see Appendix) was performed via numerical simulations. Various test orbits were propagated from a known initial condition using both sets of equations. The the resulting trajectories were then compared to verify the equivalence of the equations. The propagation were carried out using the MATLAB® *ODE*45 solver. In addition, for some test cases the trajectories were validated using the linearized solution to the Hill Equations, the Clohessy-Wiltshire (CW) equations [2]. Table 1 lists the trajectories tested as well as the resulting position and velocity errors between the Spherical and Cartesian trajectories, over the whole simulation period. The errors for all the

trajectories tested were within numerical integration errors in the order of 1×10^{-6} meters. An example of the validation trajectories, corresponding to the last row of Table 1, is shown in Figure 1 and the corresponding errors in Figure 2.

Table 1 Spherical relative motion equations validation results.

Test Description (Compared with)	IC [m & m/s] ($\mathbf{x}^c = [x\ y\ z\ \dot{x}\ \dot{y}\ \dot{z}]^T$)	$\|\|\mathbf{x}^c(t) - \mathbf{x}^s(t)\|\|$ Pos [m]	Vel [m/s]
Arbitrary IC (CW)	[100 10 150 0.01 0.1 0.2]	8.00e-08	4.77e-11
Arbitrary IC (Hill)	[100 10 150 0.01 0.1 0.2]	7.23e-08	3.86e-11
Different Altitude (CW)	[0 0 150 0.2617994 0 0]	2.31e-08	1.26e-11
Release at Z-Direction (CW)	[0 0 150 0 0 0]	7.32e-08	8.04e-11
Release at Y-Direction (CW)	[0 10 0 0 0 0]	3.31e-10	1.78e-09
Initial Velocity on X-Direction (CW)	[ε^* 0 0 0.01 0 0]	7.01e-09	6.07e-12
Initial Velocity Out of Plane (CW)	[0 ε^* 0 0 0.1 0]	9.51e-10	3.57e-10
Forced Motion with Accelerations** (Hill)	[1000 10 15 0.01 0.01 0.02]	3.84e-05	3.37e-08

*Note: ε = 2.22e-16 is used to avoid the numerical singularity at $\mathbf{r} = [0\,0\,0]^T\ m$

**Constant acceleration used throughout the simulation: $\mathbf{a} = [1\,2\,3]^T\ m/s^2$

4 In-Orbit Bearings-Only Navigation Filters

Two discrete Extended Kalman filters were formulated according to [8], using the Cartesian and Spherical equations of motion. The propagation step within the filters was implemented using a fourth order Runge-Kutta (RK4) integration of the state equations, shown below.

The state vectors for the navigation filters in Cartesian $\mathbf{x}^c$ and Spherical $\mathbf{x}^s$ coordinates are defined as in Equations 23 and 24 respectively. The state equations for each filter, $\mathbf{f}^c(\mathbf{x}^c)$ and $\mathbf{f}^s(\mathbf{x}^s)$, were formulated from the relative motion equations for circular orbits in Cartesian (18-20) and Spherical (4-6) coordinates respectively. These are shown in Equations 7 and 8 below.

$$\dot{\mathbf{x}}^c = \mathbf{f}^c(\mathbf{x}^c) = \begin{bmatrix} \dot{x} \\ \dot{y} \\ \dot{z} \\ 2\dot{z}\omega + a_x \\ -\omega^2 y + a_y \\ 3\omega^2 z - 2\dot{x}\omega + a_z \end{bmatrix} \tag{7}$$

Fig. 1 Validation Example Trajectory for the Spherical Relative Motion Equations

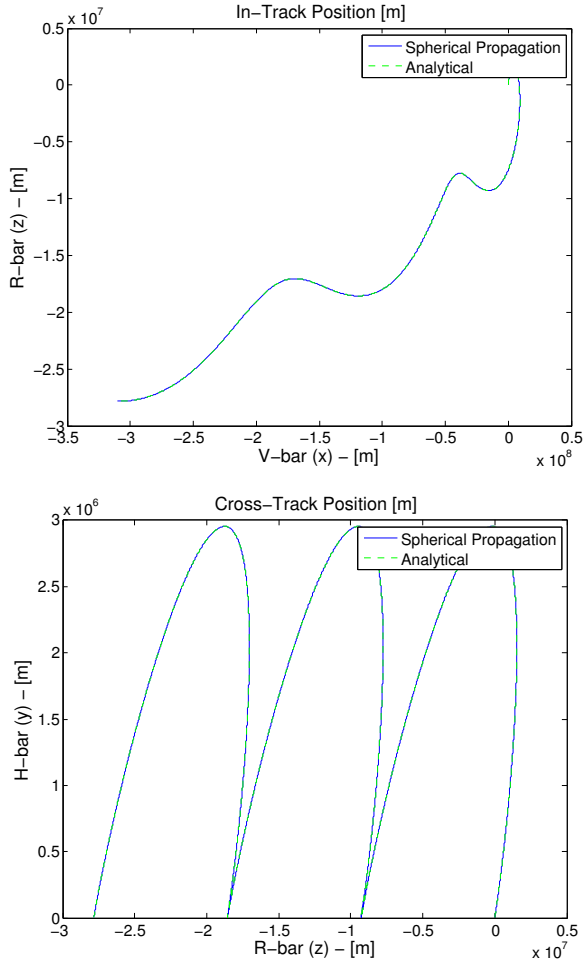

$$\dot{\mathbf{x}}^s = \mathbf{f}^s(\mathbf{x}^s) = \begin{bmatrix} \dot{r} \\ \dot{\theta} \\ \dot{\phi} \\ a_r + r\dot{\phi}^2 + 2r\dot{\phi}\omega c_\theta + r\dot{\theta}^2 c_\phi^2 + 2rs_\phi s_\theta \dot{\theta}\omega c_\phi + r\omega^2\left(c_\phi^2 c_\theta^2 - 4c_\phi^2 + 3\right) \\ \frac{a_\theta - 2\dot{r}\omega s_\phi s_\theta}{rc_\phi} + \frac{2\dot{\phi}\dot{\theta}s_\phi}{c_\phi} - \frac{2\dot{r}\dot{\theta}}{r} - c_\theta s_\theta \omega^2 - 2\dot{\phi}s_\theta\omega \\ \frac{a_\phi - 2\dot{\phi}\dot{r} - 2\dot{r}\omega c_\theta}{r} + \omega^2 s_\phi c_\phi\left(s_\theta^2 + 3\right) - \dot{\theta}^2 s_\phi c_\phi + 2\dot{\theta}\omega s_\theta c_\phi^2 \end{bmatrix} \quad (8)$$

Finally, the angles-only measurement equations for each filter were developed from the geometric relations in Figure 10. These are shown in Equation 9 and 10 for the Cartesian and Spherical filters respectively.

Fig. 2 Validation Errors for the Example Trajectory

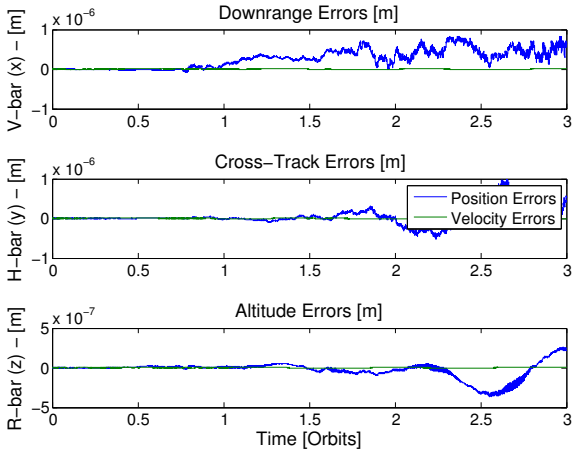

$$\mathbf{h}^c(\mathbf{x}^c) = \begin{bmatrix} \arctan(y/x) \\ \arcsin\left(z/\sqrt{x^2+y^2+z^2}\right) \end{bmatrix} \tag{9}$$

$$\mathbf{h}^s(\mathbf{x}^s) = \begin{bmatrix} \theta \\ \phi \end{bmatrix} \tag{10}$$

4.1 Filter Stability Measure

Even though the stability of Extended Kalman Filters can not be guaranteed, EKFs are attractive since their performance is near-optimal when the estimation errors are small and the non-linearities are tightly cone bounded [9]. Several references including [9] suggest that the performance of an EKF depends heavily on the coordinate system used to formulate the filter. In order to aid in the selection of a suitable coordinate system, Weiss and Moore [9] provide a "stability measure" test based on a bound on the decay rate of a Lyapunov function. According to this test, the larger the value of the "stability measure" μ_s in Equation 11, the more stable the system will be over the range of state estimates. Here, $\mathbf{R}$ is the noise covariance matrix for the measurements.

$$\mu_s = \mathbf{h}^T \mathbf{R}^{-1} \mathbf{h} - [\mathbf{H}_k \mathbf{x} - \mathbf{h}]^T \mathbf{R}^{-1} [\mathbf{H}_k \mathbf{x} - \mathbf{h}] \tag{11}$$

$$\text{where} \quad \mathbf{H}_k = \left. \frac{\partial \mathbf{h}(\mathbf{x})}{\partial \mathbf{x}^T} \right|_{\mathbf{x}=\mathbf{x}_k}$$

Applying this stability measure to both the cartesian and spherical systems by substituting the corresponding measurement equations from 9 and 10 into Equation

11, we obtain the following measures for each system, shown in equations 12 and 13.

$$\mu_s^c = 0 \tag{12}$$

$$\mu_s^s = (\mathbf{h}^s)^T \mathbf{R}^{-1} \mathbf{h}^s = \frac{\phi^2}{R_\phi} + \frac{\theta^2}{R_\theta} \tag{13}$$

Since $\mu_s^s > 0$ for any real value of $\mathbf{h}^s$, the stability measure test proposes that the spherical coordinate formulation is a better candidate for an EKF than its cartesian counterpart. Note that this is not in any way a guarantee of stability of the EKF. It is only an indicator that in the linear case, or when the filter is operating near the linearization set-point, the rate of decay of "energy" in the system for the spherical filter formulation would be positive and larger than the cartesian one. Therefore, this supports the results of the simulations that are presented in the next Section.

5 Navigation Filter Simulations

A Simulink® simulation was prepared where both the Cartesian and the Spherical filters were used to estimate a trajectory propagated using the Hill equations. The simulation model is shown in Figure 3.

Fig. 3 Simulation Model

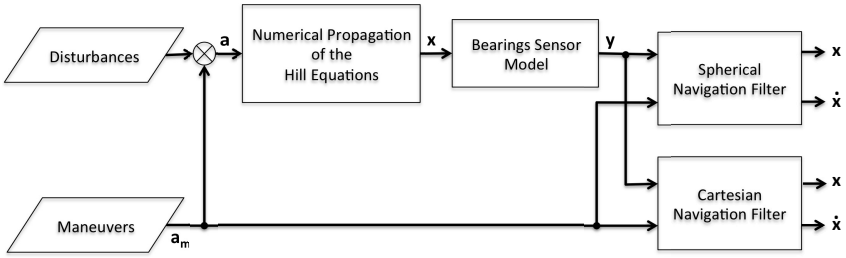

The parameters and tunings used to initialize the simulations of the navigation filters are summarized in Table 2 . It is important to note that the same tunings and initialization parameters were used for both filters by converting the cartesian quantities into spherical ones, as explained in the Appendix.

Table 2 Filter Comparison Simulation Parameters

Parameter	Description	Simulator Value	Units
Environment			
Orbital Period (T)	90 min	54000	[s]
Fly-around IC ($\mathbf{x}_0^c$)	$[xyz\dot{x}\dot{y}\dot{z}]$	[10000 5 1 0 0 -2]	[m & m/s]
Unmodelled Acceleration	100m/rev 3σ	$([100/T^2\ 100/T^2\ 100/T^2]/3)^2$	[m/s]
Time Step (T_s)	10 sec	10	[s]
Sensor			
Measurement Noise	1 mrad/axis 3σ	$([1e\text{-}3\ 1e\text{-}3]/3)^2$	[rad]
Measurement Bias	None	[0 0]	[rad]
Filters			
Spread of Initial Errors	StDev 1σ	[300 30 300 0.03 0.3 0.3]/3	[m & m/s]
Initial Covariance	300m, 0.3 m/s 3σ	$\text{diag}(([300\ 300\ 300\ 0.3\ 0.3\ 0.3]/3)^2)$	[m & m/s]
Sensor Noise Covariance	1 mrad/axis 3σ	$\text{diag}(([1e^{-3}\ 1e^{-3}]/3)^2)$	[rad]
Plant Noise Covariance	100 m/rev 3σ	$\text{diag}(([0\ 0\ 0\ 100\ 100\ 100]/3T)^2)/T_s$	[m & m/s]
Orbital Rate (ω)	$2\pi/T$	0.0012	[rad/s]
Time Step (T_s)	10 sec	10	[s]

5.1 Observability of the Bearings-Only Problem

The problem of estimating position and velocity from only angle measurements is known to have reduced observability depending on the relative motion between the satellites [10]. In addition, the range along the LOS direction is known to be not observable in the bearings-only problem, unless a maneuver is executed in a suitable direction [10].

In order to illustrate this point as well as to validate the functionality of the filters, a 'noiseless' simulation was performed. All sensor noises and un-modelled disturbances in Table 2 were set to zero. The reference trajectory was generated by propagating the following initial condition for the position and velocity $\mathbf{x_0} = [xyz\dot{x}\dot{y}\dot{z}]^T = [10000\ 5\ 1\ 0.2\ 0.1\ -2]^T$. As it can be seen on Figure 4 and 5, both filters can track the reference trajectory fairly well.

The filter covariance is also shown in Figure 4 for some points along the trajectory. These ellipses, which are the filter's estimate of its own errors, correspond to the 3σ values from the error covariance matrices, scaled by a factor of 3 for easy visualization. The covariances are very similar for both filters since they employ the same tunning of their Plant and Sensor noise covariance matrices. Finally, it can be seen that the uncertainty is always greater in the LOS direction to the target at [0,0], as there is no observability in this direction when no maneuvers are performed.

Fig. 4 Filter Comparison Trajectory

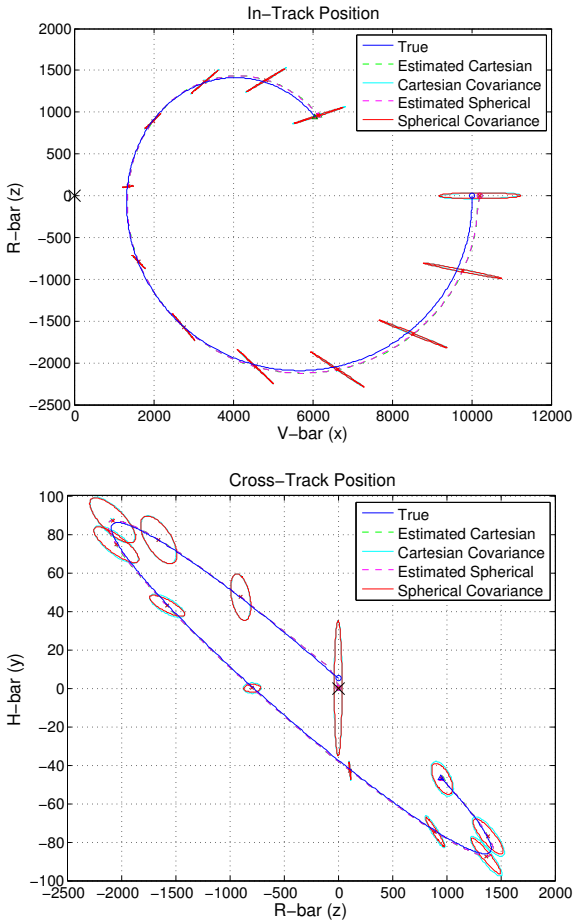

5.2 Filter Comparison Monte Carlo

One hundred Monte Carlo Simulations were run in order to test the performance of the filters over a range of different initialization errors employing noisy measurements and subject to disturbances in the reference trajectory. In order to provide a high dynamic relative motion that aids filter convergence, the relative initial conditions were chosen to yield a 'football' or 'fly-around' periodic trajectory. Table 2 in section 5 summarizes all the parameters used to initialize the Monte Carlo.

In addition, a maneuver was performed mid way through the simulation in order to show how the filters gain observability in the range direction. This impulsive maneuver was executed after two orbits via an acceleration pulse $\mathbf{a}_{man} = [0\ 0.005\ -0.005]^T$ lasting 10 seconds, resulting in a total delta-V of 0.1 m/s in the

Fig. 5 Filter Comparison Velocities

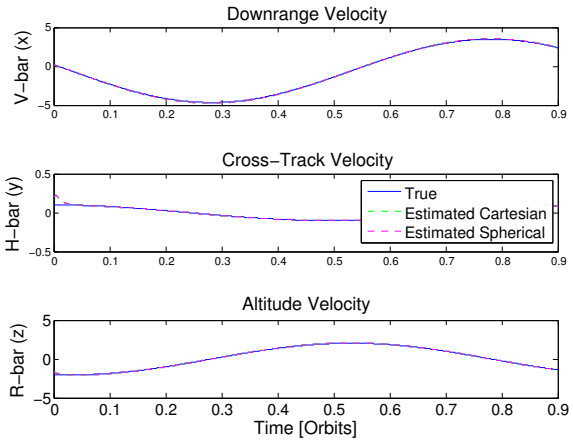

y and $-z$ directions. Figure 6 shows the resulting trajectory estimates by both filters, along with the reference trajectories for each of the Monte Carlo simulations. Note the trajectory change due to the maneuver after two orbits.

Statistical dispersions were computed from the trajectory errors of each simulation in order to evaluate the 1σ performance of each filter. These are shown in Figure 7 along with their percentage of the range to the target. This last measure is very useful in spacecraft rendezvous since, as a rule of thumb, a relative position estimate of around 1% of the range is required to achieve impulsive rendezvous [2].

Finally, the run-time of each filter was analyzed during the Monte Carlo simulations. On a 1.8 GHz computer, the cartesian filter demanded on average 8.3×10^{-4} seconds per call (propagation + update), while the spherical one demanded 9.1×10^{-4} seconds per call. That is only about a 10% increase in average CPU run time for the spherical filter.

5.3 Filter Comparison Results

The Monte Carlo analysis shows that for the reference trajectory chosen, the spherical filter statistically outperforms the cartesian one. This can be seen in the resulting navigation dispersions shown in Figure 7. Note that both solutions slowly diverge due to the inherent reduced observability of the bearings-only navigation problem. However, when a maneuver is performed in a suitable direction [10], it provides the necessary observability to reduce the estimated error in the LOS direction. Both filters take advantage of this and reduce their total estimation uncertainties when the maneuver is performed.

In any case, the spherical filter tracks the reference trajectory with superiority when no maneuvers are performed, diverging at a much slower rate. Conceptually,

Fig. 6 Monte Carlo Trajectories

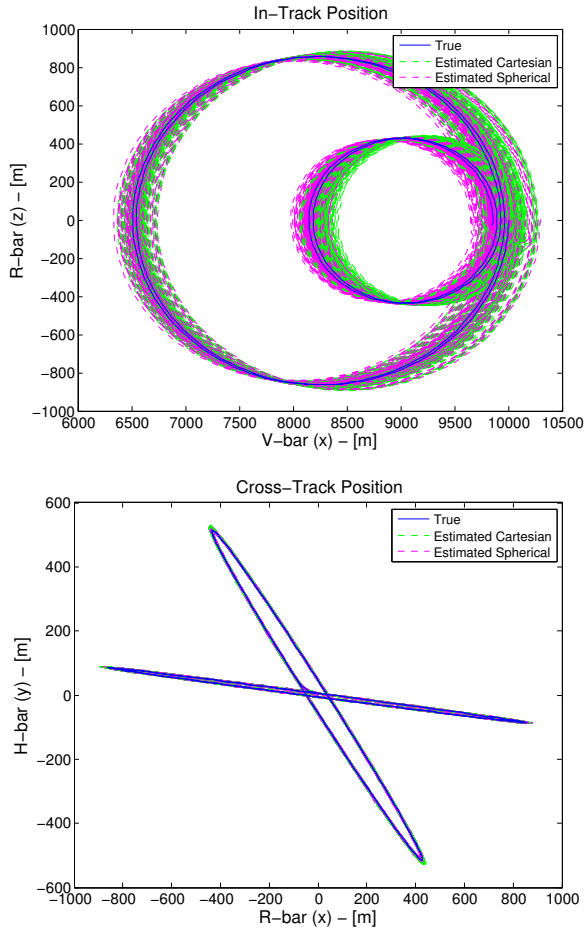

this is due to the fact that in contrast to the cartesian filter, the spherical filter separates the observable (angles) and un-observable (range) states. Essentially, it only needs to estimate the range and range-rate, as the other four states are directly the measurements and their derivatives. On the other hand, the cartesian filter needs to estimate all six states (position and velocities) from measurements that are non-linearly related to its states, resulting in lower performance. Mathematically, this is readily explained by noting where the filters employ key linearizations of the underlying equations. The Extended Kalman filter relies on a linearization of the measurement equation in order to calculate the Kalman Gain that is used to apply the measurement update. In contrast to the spherical filter where this equation is already linear, the measurement equation in the cartesian filter is highly non-linear (Refer to Equations 9 and 10). Thus, the linearization required in the cartesian filter results

Fig. 7 Monte Carlo Trajectory Dispersions

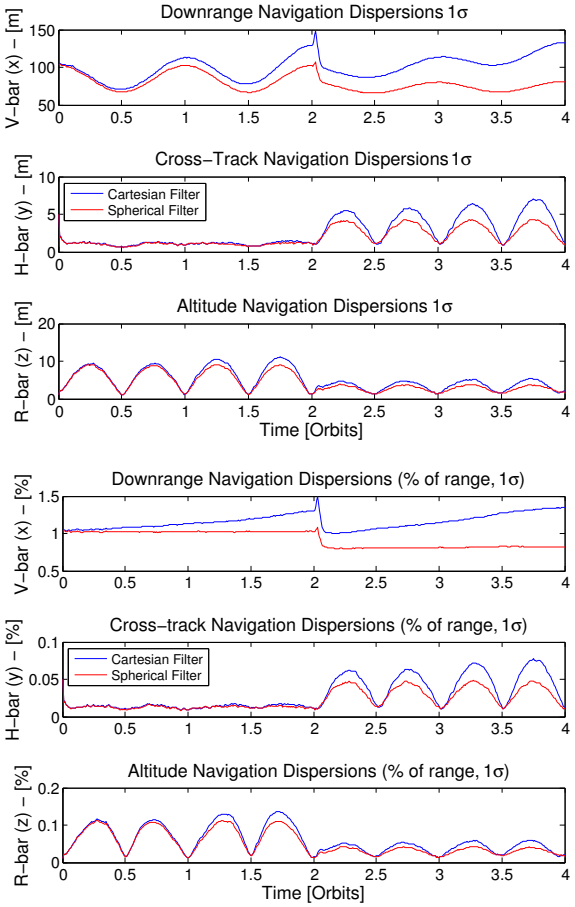

in a slightly less accurate measurement update. In addition, the linearized measurement equation is also used in the update of the filter covariance matrix, introducing further inaccuracies. Therefore, even though both filters rely on a linearized state transition matrix to propagate their covariance matrix, the cartesian filter also relies on a linearized measurement equation. This introduces additional inaccuracies compared to the the spherical filter, where the measurement equation is already linear. Hence, decoupling the observable and un-observable states results in a simple measurement equation which reduces the linearization inaccuracies in the filter.

Several other simulations on top of the Monte-Carlo analysis were performed during the characterization of the spherical filter implementation, which are not shown here due to space constraints. Nevertheless, the general observation was that the Spherical filter implementation was found to be more robust than the Cartesian

one in terms of changes to its tunning parameters as well as changes to the measurement update frequency.

Finally, as mentioned in section 5.2, the increase in performance from the spherical filter only comes with a small increase of about a 10% in CPU run-time.

6 Conclusions

In this paper, the linearized equations of relative orbital motion were derived in spherical coordinates and a new in-orbit bearings-only navigation filter was implemented using these equations.

This work shows that a spherical coordinate based filter can perform better for the bearings-only in-orbit navigation problem than a traditional Cartesian implementation. A more in depth characterization of the robustness of the spherical filter implementation with respect to different measurement errors, update frequencies and and filter tunings is required. Nevertheless, these results show the potential advantages in performance and robustness that can result from the use of a coordinate system parameterization that acquires the measurements as its own states. This results in simple measurement equations, essentially shifting the non-linearities inside the EKF from the measurement update, where linearizations are heavily relied upon, to the propagation, where the full state equations can be partly employed. This was shown in the construction of the spherical filter.

Even though this filter implementation implies more development effort due to the complex and longer equations required to model the relative motion dynamics, there is little additional on-line computational effort required to perform the actual trajectory estimation. This makes the spherical filter a very interesting robust alternative for an on-board implementation.

Acknowledgements The authors would like to thank the European Space Agency (TEC-ECN Section at ESTEC) and Thales Alenia Space France (Research and Technology/Science and Observation within the R&D department) for providing the funding that made this research possible, through the ESA Networking/Partnering Initiative (NPI) program. In addition, we would like to thank André Posh from the iFR at the University of Stuttgart for the discussions on Extended Kalman Filters and their performance.

Appendix

In-Orbit Relative Motion Background

A generic derivation of the in-orbit relative motion equations is presented here. A more detailed derivation, but focused on the Cartesian coordinate parametrization of the equations, can be found in [2] and [11].

Relative Motion in the Inertial Frame

Consider the general scenario of two point mass spacecraft subject to the effects of a central Spherical gravity field and other external accelerations. Their geometry is defined in Figure 8, where the spacecraft are denominated as a Target and a Chaser with position vectors $\mathbf{r}_t$ and $\mathbf{r}_c$ respectively. In inertial space, the relative acceleration is directly the second time derivative of the relative position vector $\ddot{\mathbf{r}}$.

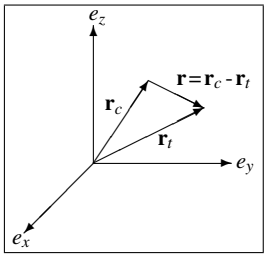

Fig. 8 Definition of the chaser, target and relative position vectors in the inertial frame

The motion of each of these spacecraft can be described by Newton's Second Law $\mathbf{F}_i = m\ddot{\mathbf{r}}_i$, where $\mathbf{F}_i$ must include all external forces for each vehicle. Considering only the influence of a central gravity force given by Newton's law of Gravitation as well as control thrust accelerations from the chaser vehicle $\mathbf{a}_{ext} = \mathbf{F}_{ext}/m_c$, the linearized differential equation for relative motion in the inertial frame is:

$$\ddot{\mathbf{r}} = \left.\frac{d\mathbf{f}_\mathbf{g}(\mathbf{r}_i)}{d\mathbf{r}_i}\right|_{\mathbf{r}_i=\mathbf{r}_t} \mathbf{r} + \mathbf{a}_{ext} \tag{14}$$

where the jacobian of $\mathbf{f}_\mathbf{g}(\mathbf{r}_i)$ comes from the linearization by Taylor expansion of the gravitational force of the chaser around the target location, which expressed with respect to a generic vector $\mathbf{r}_i = [x_i\ y_i\ z_i]^T$ is as follows:

$$\frac{d\mathbf{f}_\mathbf{g}(\mathbf{r}_i)}{d\mathbf{r}_i} = \frac{\mu}{r_i^3}\begin{bmatrix} \frac{3x_i^2}{r_i^2}-1 & \frac{3x_iy_i}{r_i^2} & \frac{3x_iz_i}{r_i^2} \\ \frac{3x_iy_i}{r_i^2} & \frac{3y_i^2}{r_i^2}-1 & \frac{3y_iz_i}{r_i^2} \\ \frac{3x_iz_i}{r_i^2} & \frac{3y_iz_i}{r_i^2} & \frac{3z_i^2}{r_i^2}-1 \end{bmatrix} \tag{15}$$

where $r_i = \sqrt{x_i^2+y_i^2+z_i^2}$.

Relative Motion in the Local Orbital Frame

The Local Orbital Frame ($\mathfrak{F}^{\mathbf{lo}}$), fixed to the orbital motion of the target spacecraft, is centered at the target position $\mathbf{r}_t$ and rotates with respect to the inertial frame at a rate $\boldsymbol{\omega}$ equal to the instantaneous orbital rate of the target, as depicted in Figure

9. Here, the z-axis always points towards the center of the orbit; the y-axis is in the opposite direction of the angular momentum and the x-axis completes the triad.

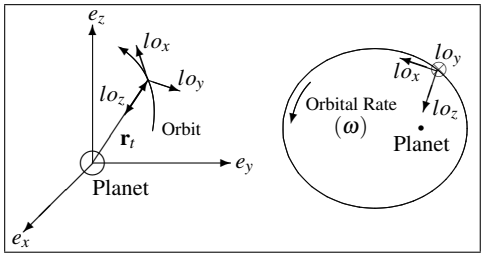

Fig. 9 Definition of the local orbital frame $\left(\mathfrak{F}^{\mathbf{lo}}\right)$

In order to obtain the equations of relative motion in the $\mathfrak{F}^{\mathbf{lo}}$ frame, Equation 14 can be expressed in this frame by using the second derivative of the relative position vector $\mathbf{r}$ in the rotating frame:

$$\ddot{\mathbf{r}}^{lo} + 2\boldsymbol{\omega} \times \dot{\mathbf{r}}^{lo} + \dot{\boldsymbol{\omega}} \times \mathbf{r}^{lo} + \boldsymbol{\omega} \times \boldsymbol{\omega} \times \mathbf{r}^{lo} - \left.\frac{d\mathbf{f}_{\mathbf{g}}(\mathbf{r}_i)}{d\mathbf{r}_i}\right|_{\mathbf{r}_i = \mathbf{r}_t^{lo}} \mathbf{r}^{lo} = \mathbf{a}_{ext}^{lo} \tag{16}$$

In addition, from the definition of the $\mathfrak{F}^{\mathbf{lo}}$ frame, the following assumptions apply to Equation 16:

$$\mathbf{r}_{\mathbf{t}}^{\mathbf{lo}} = \begin{bmatrix} 0 \\ 0 \\ -r_t \end{bmatrix}, \quad \boldsymbol{\omega} = \begin{bmatrix} 0 \\ -\omega \\ 0 \end{bmatrix}, \quad h = {r_t}^2 \omega \quad \text{and} \quad k = \frac{\mu}{h^{\frac{3}{2}}} \tag{17}$$

where the constant h is the orbital momentum for the planar orbital motion of the target spacecraft and the constant k is defined as done in [11] in order to remove the orbital radius r_t from the equations.

The Hill Equations

The Hill equations, shown below, can be obtained by substituting into Equation 16 the assumptions related to a cartesian position vector $\mathbf{r} = [x\ y\ z]^T$ along with the assumptions for circular orbits described in Section 2.

$$\ddot{x} = a_x + 2\,\omega\,\dot{z} \tag{18}$$

$$\ddot{y} = a_y - \omega^2\, y \tag{19}$$

$$\ddot{z} = 3\,z\,\omega^2 - 2\,\dot{x}\,\omega + a_z \tag{20}$$

Definition of the Spherical Coordinates

In the $\mathfrak{F}^{\mathbf{lo}}$ frame, we can define the relative position vector in terms of the Spherical coordinates r, θ and ϕ as shown in Figure 10.

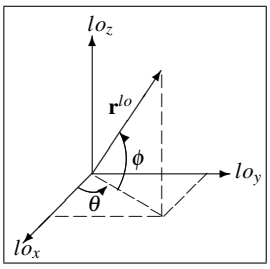

Fig. 10 Definition of the Relative Position Vector in terms of the Spherical Coordinates in the $\mathfrak{F}^{\mathbf{lo}}$ frame

The relative position vector in terms of these Spherical coordinates is:

$$\mathbf{r}^{lo} = \begin{bmatrix} x \\ y \\ z \end{bmatrix} = \begin{bmatrix} rc_\phi c_\theta \\ rc_\phi s_\theta \\ rs_\phi \end{bmatrix} \tag{21}$$

where $c_i = \cos(i)$ and $s_i = \sin(i)$ for $i = \phi$ or θ is used to simplify the notation. It is also useful to express the external accelerations $\mathbf{a}^{lo}_{ext}$ in terms of the spherical variables $\mathbf{a}^{lo}_{sph} = \begin{bmatrix} a_r \; a_\theta \; a_\phi \end{bmatrix}^T$:

$$\mathbf{a}^{lo}_{ext} = \mathbf{C_{sc}}^T \mathbf{a}^{lo}_{sph} \quad \text{where} \quad \mathbf{C_{sc}} = \begin{bmatrix} c_\phi c_\theta & c_\phi s_\theta & s_\phi \\ -s_\theta & c_\theta & 0 \\ -c_\theta s_\phi & -s_\phi s_\theta & c_\phi \end{bmatrix} \tag{22}$$

Coordinate Transformations

In order to compare the Spherical coordinate results with the Cartesian ones, the following coordinate transformations were defined. These were used to compute the equivalent initial conditions in Spherical coordinates as well as to translate the resulting trajectories to Cartesian coordinates. Each position-velocity vector expressed in Cartesian $\mathbf{x}^c_i$ or Spherical coordinates $\mathbf{x}^s_i$, can be transformed back and forth between the coordinate systems by using the relationships in Equations 23 and 24. These relations were obtained from the geometric definitions of Figure 10 as well as their time derivatives.

$$\mathbf{x}_i^c = \begin{bmatrix} x \\ y \\ z \\ \dot{x} \\ \dot{y} \\ \dot{z} \end{bmatrix} \equiv \mathbf{F}_{cs}(\mathbf{x}_i^s) = \begin{bmatrix} rc_\phi c_\theta \\ rc_\phi s_\theta \\ rs_\phi \\ \dot{r}c_\phi c_\theta - r\dot{\theta}c_\phi s_\theta - \dot{\phi}rc_\theta s_\phi \\ \dot{r}c_\phi s_\theta - \dot{\phi}rs_\phi s_\theta + r\dot{\theta}c_\phi c_\theta \\ \dot{r}s_\phi + \dot{\phi}rc_\phi \end{bmatrix} \tag{23}$$

$$\mathbf{x}_i^s = \begin{bmatrix} r \\ \theta \\ \phi \\ \dot{r} \\ \dot{\theta} \\ \dot{\phi} \end{bmatrix} \equiv \mathbf{F}_{sc}(\mathbf{x}_i^c) = \begin{bmatrix} \sqrt{x^2+y^2+z^2} \\ \arctan\left(\frac{y}{x}\right) \\ \arcsin\left(z/\sqrt{x^2+y^2+z^2}\right) \\ \frac{x\dot{x}+y\dot{y}+z\dot{z}}{\sqrt{x^2+y^2+z^2}} \\ \frac{x\dot{y}-\dot{x}y}{x^2+y^2} \\ \frac{\dot{z}x^2-\dot{x}zx+\dot{z}y^2-\dot{y}zy}{\sqrt{1-\frac{z^2}{x^2+y^2+z^2}}\left(x^2+y^2+z^2\right)^{\frac{3}{2}}} \end{bmatrix} \tag{24}$$

Note that the singularity arising when x and y are *zero* in the calculation of θ and $\dot{\theta}$ can be resolved by using the *atan*2 function. The velocities $\dot{r}$, $\dot{\theta}$ and $\dot{\phi}$ are then solved for using the expressions in Equation 23. The covariance matrices can be transformed back and forth between the coordinate systems via a similarity transformation [12]. For example, to convert a Cartesian covariance matrix $\mathbf{P}_i^c$ into a spherical one $\mathbf{P}_i^s$, the transformation is as follows:

$$\mathbf{P}_i^s = \mathbf{M}_{sc}\,\mathbf{P}_i^c\,\mathbf{M}_{sc}^T \quad \text{where} \quad \mathbf{M}_{sc} = \left.\frac{d\mathbf{F}_{sc}(\mathbf{x}^c)}{d\mathbf{x}^c}\right|_{\mathbf{x}^c=\mathbf{x}_i^c}$$

where the matrix $\mathbf{M}_{sc}$ is the Jacobian of the transformation function $\mathbf{F}_{sc}$ in Equation 24 with respect to the cartesian coordinates $\mathbf{x}^c = [x\ y\ z\ \dot{x}\ \dot{y}\ \dot{z}]$, evaluated at the corresponding position-velocity point $\mathbf{x}_i^c$ where the covariance matrix is sampled. The inverse transformation is constructed in a similar way, using the transformation function $\mathbf{F}_{cs}$ in Equation 23.

Finally, the accelerations can be transformed back and forth betwen the cartesian $[a_x\ a_y\ a_z]$ and spherical $\left[a_r\ a_\theta\ a_\phi\right]$ representations via the simple rotation matrix defined in Equation 22.

References

1. Woffinden, D. C., *Angles-Only Navigation for Autonomous Orbital Rendezvous*, Ph.D. thesis, Utah State University, 2008.
2. Fehse, W., *Automated Rendezvous and Docking of Spacecraft*, Cambridge Aerospace Series, Cambridge University Press, 2003.
3. Petridis, V., "A method for bearings-only velocity and position estimation," *IEEE Transactions on Automatic Control*, Vol. 26, No. 2, April 1981, pp. 488–493.
4. Hammel, S. E., Liu, I. P. T., Hilliard, J. E., and Gong, K. E., "Optimal observer motion for localization with bearing measurements," *Computers Math. Applic.*, Vol. 18, No. 1-3, 1989,

pp. 171–180.
5. Oshman, Y. and Davidson, P., "Optimization of Observer Trajectories for Bearings-Only Target Localization," *IEEE Transactions On Aerospace And Electronic Systems*, Vol. 35, No. 3, 1999.
6. Aidala, V. j. and Hammel, S. E., "Utilization of Modified Polar Coordinates for Bearings-Only Tracking," *IEEE Transactions on Automacit Control*, Vol. AC-28, No. 3, 1983, pp. 283–294.
7. Mallick, M., Arulampalam, S., Mihaylova, L., and Yan, Y., "Angle-only Filtering in 3D using Modified Spherical and Log Spherical Coordinates," *Proceedings of the 14th International Conference on Information Fusion*, Chicago, USA, 2011, pp. 1905–1912.
8. Gelb, A., *Applied Optimal Estimation*, MIT Press, 1974.
9. Weiss, H. and Moore, J. B., "Improved Extended Kalman Filter Design for Passive Tracking," *IEEE Transactions on Automatic Control*, Vol. AC-25, No. 4, 1980.
10. Woffinden, D. C. and Geller, D. K., "Optimal Orbital Rendezvous Maneuvering for Angles-Only Navigation," *Journal of Guidance, Control, and Dynamics*, Vol. 32, No. 4, July 2009, pp. 1382–1387.
11. Yamanaka, K. and Ankersen, F., "New State Transition Matrix for Relative Motion on an Arbitrary Elliptical Orbit," *Journal of Guidance, Control, and Dynamics*, Vol. 25, No. 1, Jan. 2002, pp. 60–66.
12. Vallado, D. A., "Covariance Transformations for Satellite Flight Dynamics Operations," *AAS / AIAA Astrodynamics Specialist Conference*, Big Sky, Montana, 2003, pp. 1–35.